Low magnetic field induced giant magnetoelectric coupling in Cu^{2+}-doped *Y*-type $BaSrCo_{2-x}Cu_xFe_{11}AlO_{22}$ stemming from enhanced superexchange interaction

Dongpeng Zhao,[1,2] Jun Li,[1,2,*] Tongtong Xu,[1,2] Huantong Wu,[1,2] Xiping Chen,[3] Guangai Sun,[3] and Zhongxiang Zhou[1,2,†]

[1]*School of Physics, Harbin Institute of Technology, Harbin 150001, China*

[2]*Heilongjiang Provincial Key Laboratory of Plasma Physics and Application Technology, Harbin Institute of Technology, Harbin 150001, China*

[3]*Key Laboratory for Neutron Physics of CAEP, Institute of Nuclear Physics and Chemistry, Mianyang 621999, China*

(Received 16 November 2022; revised 29 August 2023; accepted 25 October 2023; published 28 November 2023)

A giant, reversible magnetoelectric polarization induced under one order of magnitude lower magnetic field was observed in *Y*-type $BaSrCo_{2-x}Cu_xFe_{11}AlO_{22}$ $(0 < x < 1)$ ceramics. When increasing Co^{2+} cations are substituted with Cu^{2+}, the saturation magnetization decreases and the flipping electric polarization accompanied with an attenuation feature is gradually frustrated. Samples' insulation degree and magnetodielectric response together with the superexchange interaction between magnetic moments of $\bar{\mu}_L$ and $\bar{\mu}_S$ are all enhanced for the moderately doped Cu^{2+} $(x = 0.5)$, which contributes to the excellent magnetoelectric coupling performances in $BaSrCo_{1.5}Cu_{0.5}Fe_{11}AlO_{22}$ with a giant magnetoelectric current of 23 $\mu A/m^2$, magnetoelectric polarization of 35 $\mu C/m^2$, and huge magnetoelectric coupling coefficients of 4496 ps/m. Furthermore, the magnetoelectric polarization can be tuned by switching angles between the direction of the surfaces of the electrodes and the external magnetic field. Such a giant magnetoelectric polarization under so low magnetic field and reversibility make the multiferroic material system promising in real world applications in conceiving and developing nonvolatile memory and new functional devices.

DOI: 10.1103/PhysRevB.108.184430

I. INTRODUCTION

Magnetoelectric multiferroics possess both magnetism and ferroelectricity, offering a good opportunity for coupling between electric polarization (*P*) and magnetization (*M*) [1]. The enhancement of coupling strength between *P* and *M* of multiferroics is a subject of keen interest for both their intriguing fundamental physics and their potential applications in the fields of nonvolatile memory and new functional devices [2].

The ferroelectric and magnetic orders of single-phase multiferroics, both from spin orders, usually exhibit strong magnetoelectric coupling [3,4]. *Y*-type hexaferrites with tunable magnetic structures are potential single-phase multiferroics with magnetoelectric coupling effects [5]. *Y*-type hexaferrites possess the $A_2Me_2Fe_{12}O_{22}$ chemical formula, where *A* and *Me* denote an alkaline-earth-metal ion and a divalent metal ion, respectively [6].

Previous studies suggest that there are several key factors behind the magnetoelectric (ME) properties of *Y*-type $A_2Me_2Fe_{12}O_{22}$ hexaferrites, such as annealing process, sintering temperature, and ions substitution. The ions substitution approach has been proven to be an effective way to modify the magnetoelectric performances of *Y*-type hexaferrites [6–12]. Ishiwata *et al.* reported that the Mg element completely substituted for Zn in $Ba_2Zn_2Fe_{12}O_{22}$ could effectively reduce the external magnetic field to several dozen mT and then induce the ceramic's magnetoelectric polarization [6]. Incresing the Co element is able to enhance the ceramic's resistivity, which in turn enhances the ceramic's *ME* performance [8]. Doping the Sr element can obviously affect the superexchange interaction between magnetic moments [9]. The introduction of Zn is able to change hexaferrites' magnetic transition temperature [10]. The approach of Al substitution in *Y*-type $Ba_{0.5}Sr_{1.5}Zn_2Fe_{12}O_{22}$ (BSZFO) increased the material's magnetoelectric susceptibility [11]. In addition, the Al substitution scheme has been proven to be an effective route to enhance magnetoelectric susceptibility and stabilize the nonreversal ferroelectric polarization of $BaSrCo_2Fe_{11}AlO_{22}$ reported by Hirose *et al.* [12]. Therefore, proper ions substitution in *Y*-type hexaferrites can improve a material's magnetoelectric performance.

CuO as a fluxing agent plays an important role in enhancing the ceramic's density, further reducing the material's leakage current, which is beneficial for the improvement of the material's magnetoelectric performance. Therefore, to further modify the ceramic's magnetoelectric performance, introducing CuO in *Y*-type hexaferites may be an effective approach. Based on this consideration, in this work, Cu^{2+} cations were introduced in *Y*-type $BaSrCo_{2-x}Cu_xFe_{11}AlO_{22}$ by us and their impact on magnetoelectric coupling was systemically investigated.

II. EXPERIMENTAL METHODS

Y-type hexaferrite $BaSrCo_{2-x}Cu_xFe_{11}AlO_{22}$ was prepared by traditional solid state reaction methodology [13]. The

*Corresponding author: lijuna@hit.edu.cn
†Corresponding author: zhouzx@hit.edu.cn

starting materials were high-purity $BaCO_3$, $SrCO_3$, Co_3O_4, CuO, Fe_2O_3, and Al_2O_3, which were purchased from Aladdin (Shanghai). Raw materials were weighted with stoichiometry ratio and dispersed in ethanol for thorough mixing and then ground in a planetary ball mill for about 12 h [14]. The well mixed liquid material was then laid in the drying oven to get eliminate the ethanol by natural evaporation. The dried materials were then put into a box-type furnace in a curbic container for presintering for about 10 h [15]. The presintered materials were again well mixed and ground, and then pressed into pellets with a diameter of 8 mm and thickness of 1 mm for sintering. The pellets were sintered in a tube-type furnace within the temperature range of 1115-1230 °C for 10 h. In the sintering process, the oxygen atmosphere was maintained to improve the ceramic's resistivity. The x-ray diffraction (XRD) within the Cu $K\alpha$ radiation source in the range of $2\theta = 10$–$90°$ was taken to determine the crystal's structure as well as quality [16]. A scanning electron microscope (SEM) and an energy dispersive spectrometer (EDS) were applied for sample morphology and composition characterization. To that end, the sintered pellets were cut into a rectangular shape with a thickness of 0.2–0.3 mm and a surface area of about 5 mm^2 for characterization of the magnetic, electric, dielectric, and magnetoelectric performances. The magnetization was measured with a vibrating sample magnetometer (Lake Shore, 7407) [17]. Magnetic, dielectric, and magnetoelectric coupling properties were obtained by using a homemade system consisting of *LCR*, an electrometer (model 6517B, Keithley), a lock-in amplifier, an electromagnet (Oriental Jingchen Co., Ltd.), a physical property measurement system (Dynacool-14T), and a radiant technologies precision multiferroic system (Radiant Technologies, Inc.) Ceramics were poled before the magnetoelectric coupling measurements. The magnetoelectric current (I) was measured through tuning scanning external magnetic field, which was generated by an electromagnet controlled by a DC power supply. The system was controlled by a program compiled by LABVIEW software [18,19].

III. RESULTS AND DISCUSSION

A. Morphology, ferroelectric, and magnetic characterization of $BaSrCo_{2-x}Cu_xFe_{11}AlO_{22}$

The crystal structures of $BaSrCo_{2-x}Cu_xFe_{11}AlO_{22}$ can be considered as alternating stacks of magnetic T and S blocks with a proper-screw-type rotation as shown in Figs. 1(c)–1(f) [20]. The XRD in Fig. 1(a) suggests features of Y-type hexaferrites with space group $R\bar{3}m$ [21]. The diffraction peaks (see Supplemental Material Fig. S1 [22]) exhibits a right-shifted trend with increasing Cu^{2+} demonstrating that the lattice volume decreases with introducing Cu^{2+}. During the sintering process, the adequate sintered temperature gradually decreased with the increase of Cu^{2+}: 1230 °C ($x = 0$) > 1220 °C ($x = 0.1$) > 1190 °C ($x = 0.3$) > 1175 °C ($x = 0.5$) > 1140 °C ($x = 0.7$) > 1115 °C ($x = 0.9$), respectively (see Supplemental Material Fig. S2 [22]). Such a trend can be attributed to the fluxing function of CuO, lowering the ceramic's melting point, which is expedient to raise the density of prepared hexaferrites [23]. The elements Ba, Sr, Co, Cu, Fe, Al, and O were nearly in uniform distribution

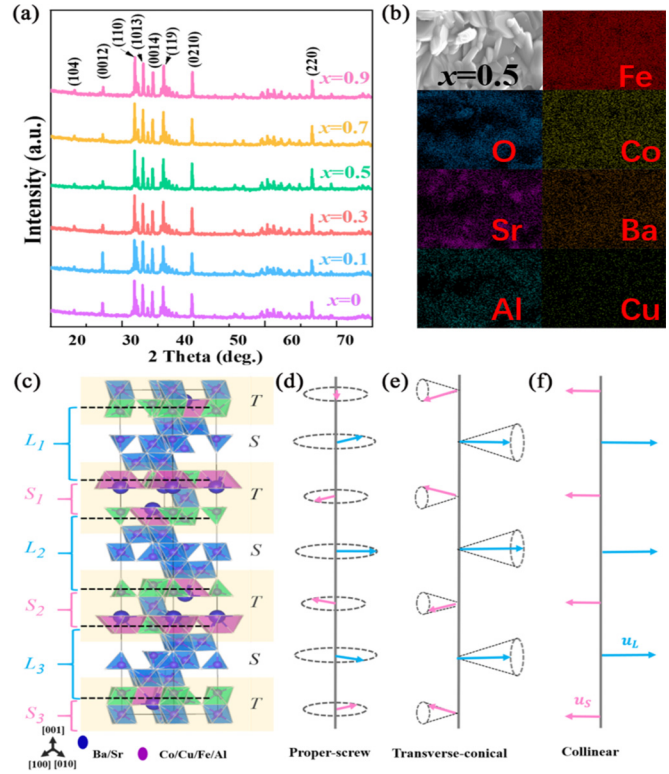

FIG. 1. (a) The XRD of $BaSrCo_{2-x}Cu_xFe_{11}AlO_{22}$. (b) The morphology and elements distribution of $BaSrCo_{1.5}Cu_{0.5}Fe_{11}AlO_{22}$. (c) Schematic crystal structures of Y-type $BaSrCo_{2-x}Cu_xFe_{11}AlO_{22}$. The magnetic structures consist of alternate stacks of T blocks and S blocks, respectively. Illustrations of magnetic structures with (d) the proper screw magnetic structure, (e) the transverse-conical magnetic structure, and (f) the collinear magnetic structure.

and the ceramic's morphology points to obvious hexagonal sheet structures based on the SEM results in Fig. 1(b) and Supplemental Material Fig. S3 [22]. The mapping results showed that the contents of Cu^{2+} and Co^{2+} conformed to the stoichiometric ratio with x changed from 0 to 0.9 (see Supplemental Material Fig. S2 and Table S1 [22]). It can be concluded that the samples were stoichiometric considering the uncertainties of the EDS technique [24]. The prepared high-quality ceramics is favorable to excellent magnetoelectric performances.

The dielectric constants of $BaSrCo_{2-x}Cu_xFe_{11}AlO_{22}$ in Fig. 2(a) and Supplemental Material Fig. S4 [22] show a rising trend with temperature while a falling trend with frequencies.

The collected dielectric losses of $BaSrCo_{2-x}Cu_xFe_{11}AlO_{22}$ under high frequency were low (see Supplemental Material Figs. S5 and S6 [22]), which is desirable for the material's magnetoelectric uses. Therefore, the highest frequency of 300 kHz has been selected for magnetoelectric performances tests. The dielectric peaks were not seen in the temperature range from 78 to 500 K, which demonstrates that all the investigated ceramics can keep their ferroelectric performances up to 500 K, which can guarantee the specimen's magnetoelectric coupling performance above room temperature.

The magnetic transition temperature (T_1/T_2) of $BaSrCo_{1.5}Cu_{0.5}Fe_{11}AlO_{22}$ was around 300 K as exhibited

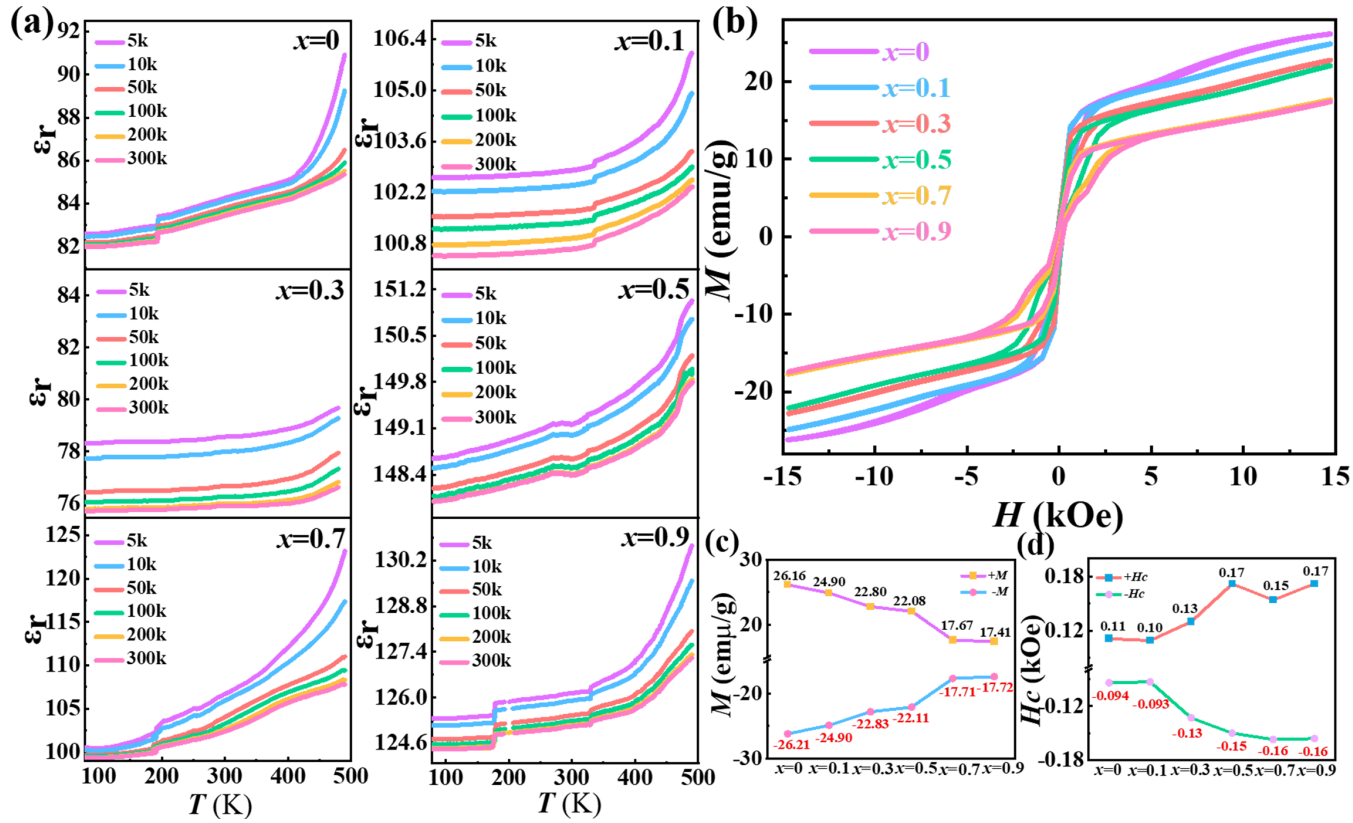

FIG. 2. (a) The dielectric temperature measurements of $BaSrCo_{2-x}Cu_xFe_{11}AlO_{22}$ under different frequencies. (b) The magnetization of $BaSrCo_{2-x}Cu_xFe_{11}AlO_{22}$ ceramics. (c) The saturation magnetization of $BaSrCo_{2-x}Cu_xFe_{11}AlO_{22}$. (d) The coercive fields of $BaSrCo_{2-x}Cu_xFe_{11}AlO_{22}$.

in Fig. 3(b), which benefits the samples' magnetoelectric coupling performance around room temperature. The magnetic Curie temperature (T_0) of $BaSrCo_{1.5}Cu_{0.5}Fe_{11}AlO_{22}$ is around 700 K, which is in accordance with other reported *Y*-type hexaferrites [25].

As exhibited in Figs. 2(b) and 2(c), the saturation magnetization intensity decreases with increasing doped Cu^{2+}. It is seen that magnetization saturates more easily when the external magnetic field was parallel rather than perpendicular to the surface of $BaSrCo_{2-x}Cu_xFe_{11}AlO_{22}$ (see Supplemental Material Fig. S7 [22]). Therefore, the sintered pellets exhibit magnetic anisotropy, which is desirable in tuning of the material's magnetic performance through applying an external magnetic field. The saturation magnetization of $BaSrCo_{2-x}Cu_xFe_{11}AlO_{22}$ under the aforementioned condition exhibits a decreasing trend: 26.157emu/g ($x = 0$) > 24.897 emu/g ($x = 0.1$) > 22.794 emu/g ($x = 0.3$) > 22.082 emu/g ($x = 0.5$) > 17.667 emu/g($x = 0.7$) > 17.413 emu/g ($x = 0.9$), respectively, in Fig. 2(c) and Supplemental Material Table S2 [22].

The decreasing magnetization can be attributed to more Co^{2+} cations being substituted by Cu^{2+}, which reduces the total magnetic moments of $BaSrCo_{2-x}Cu_xFe_{11}AlO_{22}$. It is seen that $BaSrCo_{2-x}Cu_xFe_{11}AlO_{22}$ exhibits small coercive fields and soft magnetic behaviors in Fig. 2(d), which are pivotal for inducing magnetoelectric coupling performance in

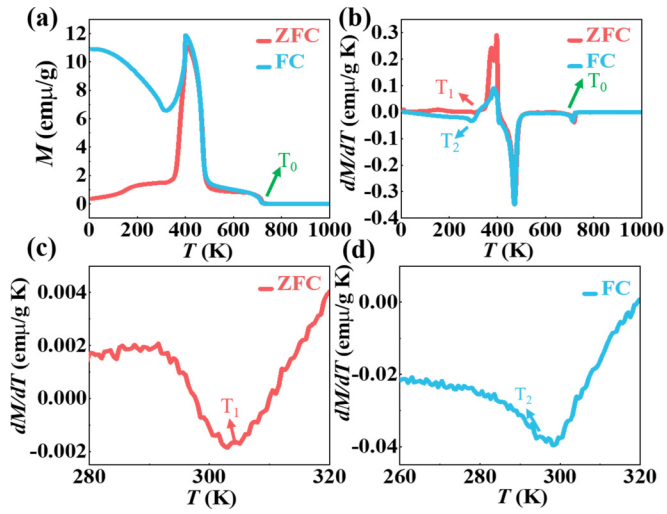

FIG. 3. (a) Magnetization of $BaSrCo_{1.5}Cu_{0.5}Fe_{11}AlO_{22}$ as a function of temperature with a measuring field of 500 Oe. (b) Temperature dependence of the derivative of magnetization to temperature ($d_M/d_T - T$) by the zero field cooling (ZFC) and field cooling (FC) processes. T_0 represents the magnetic Curie temperature and T_1/T_2 represent the magnetic transition temperature from the $d_M/d_T - T$ curves corresponding to the ZFC and FC processes. (c) The enlarged curve of $d_M/d_T - T$ by the ZFC process. (d) The enlarged curve of $d_M/d_T - T$ by the FC process.

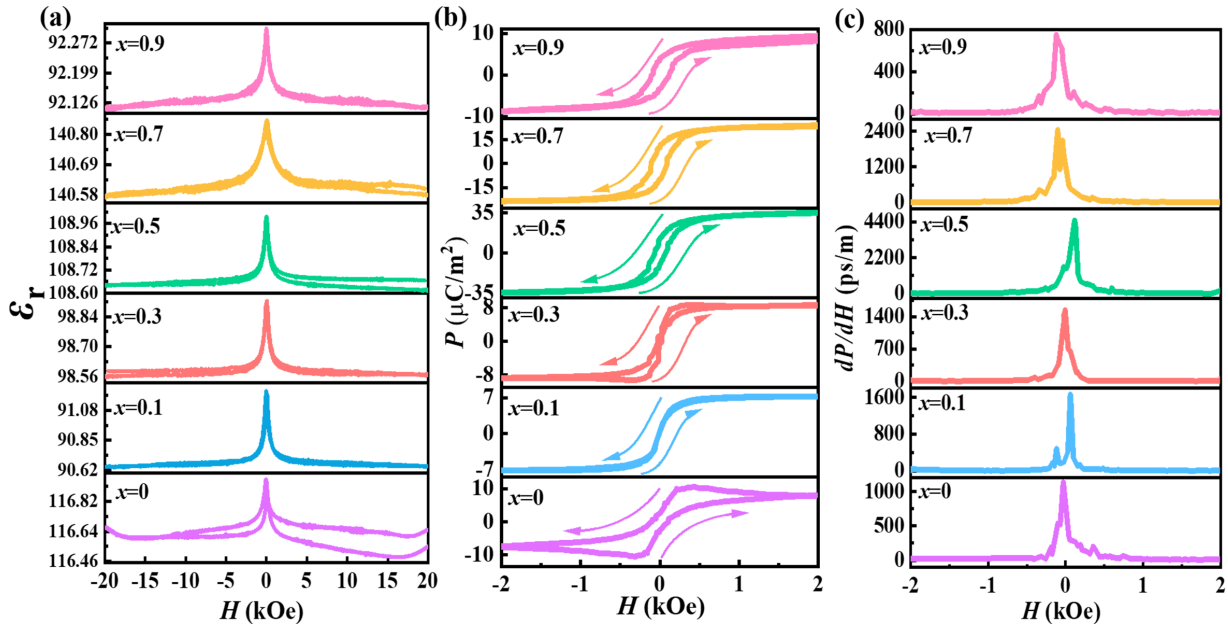

FIG. 4. (a) The magnetodielectric response of $BaSrCo_{2-x}Cu_xFe_{11}AlO_{22}$. (b) The reversal of magnetoelectric polarization of $BaSrCo_{2-x}Cu_xFe_{11}AlO_{22}$. (c) The magnetoelectric coupling coefficients of $BaSrCo_{2-x}Cu_xFe_{11}AlO_{22}$.

low magnetic fields. Meanwhile, the coercive fields show an increasing trend with increasing Cu^{2+}.

It is known that magnetization can well reflect the changing magnetic structures of $BaSrCo_{2-x}Cu_xFe_{11}AlO_{22}$ under the influence of external magnetic fields. As shown in the magnetization hysteresis loops of the as-prepared $BaSrCo_{2-x}Cu_xFe_{11}AlO_{22}$, the magnetization intensity rose rapidly with increasing external magnetic fields ranging from 0 to 2 kOe in Fig. 2(b), demonstrating that the magnetic structures of the prepared ceramics are in a noncollinear magnetic phase, which can generate ferroelectricity. The magnetization increased slowly to the saturation state at high magnetic field regions (2–15 kOe), demonstrating that the magnetic structures in such regions were of collinear ferromagnetic state. Such a state would not generate ferroelectricity. One can see that the hysteresis loops exhibit smooth and closed features accompanied with soft magnetic characteristics which can be attributed to the ferrimagnetic nature of *Y*-type $BaSrCo_{2-x}Cu_xFe_{11}AlO_{22}$ [9,26]. In the process of magnetization approaching to saturation state, the transition exhibited different characteristics with increasing Cu^{2+}. For example, for $x = 0.7/0.9$, the *M-H* loops presented nearly three steps toward magnetization state, while for $x = 0.1/0.2$, the *M-H* loops showed nearly two steps toward saturation magnetization state. Apparently, doping Cu^{2+} obviously tunes the hexaferrites' magnetic structures from the nonmonotonical process to its magnetization saturation state.

B. Magnetoelectric coupling of $BaSrCo_{2-x}Cu_xFe_{11}AlO_{22}$

Magnetodielectric constant ε of $BaSrCo_{2-x}Cu_xFe_{11}AlO_{22}$ was sensitive to an external magnetic field and an obvious magnetodielectric response occurred at 78 K under 300 kHz in Fig. 4(a) around zero magnetic field. Such behaviors were evidence that magnetoelectric coupling occurred in $BaSrCo_{2-x}Cu_xFe_{11}AlO_{22}$. Magnetodielectric (MD) responses can be used to precisely evaluate the ceramic's ε responses degree to external magnetic fields [27–29].

$$\mathrm{MD}(\%) = \frac{\Delta\varepsilon}{\varepsilon(-20\ \mathrm{kOe})}, \tag{1}$$

$$\Delta\varepsilon = \varepsilon(0\ \mathrm{kOe}) - \varepsilon(-20\ \mathrm{kOe}). \tag{2}$$

Here $\Delta\varepsilon$ is the relative change in ε. $\varepsilon(0$ kOe) and $\varepsilon(-20$ kOe) represent the dielectric constants of $BaSrCo_{2-x}Cu_xFe_{11}AlO_{22}$ in magnetic fields of 0 and -20 kOe. It is seen that $\Delta\varepsilon$ exhibited a large response around zero magnetic field, which demonstrated the existence of ferroelectric polarization [29]. One sees that $BaSrCo_{2-x}Cu_xFe_{11}AlO_{22}$ exhibited sharp dielectric peaks around zero magnetic field, indicating the boundary of ferroelectric states, suggesting that the ceramic's magnetic structures transitioned from a collinear ferromagnetic phase at high magnetic field to a noncollinear magnetic phase at low magnetic field. Although similar magnetodielectric behaviors were observed in $BaSrCo_{2-x}Cu_xFe_{11}AlO_{22}$, the MD responses varied with the difference of Cu^{2+}. The MD responses of $BaSrCo_{2-x}Cu_xFe_{11}AlO_{22}$ intially increased under $x < 0.5$ rather than $BaSrCo_2Fe_{11}AlO_{22}$. Once the doped Cu^{2+} was over 0.5, the MD responses of $BaSrCo_{2-x}Cu_xFe_{11}AlO_{22}$ were weaker than $BaSrCo_2Fe_{11}AlO_{22}$ as shown in Table I. This means that introducing Cu^{2+} can effectively tune the MD responses of $BaSrCo_{2-x}Cu_xFe_{11}AlO_{22}$.

The magnetodielectric losses (ML) can be defined by the following expression [29]:

$$\mathrm{ML} = \frac{\tan\sigma(B) - \tan\sigma(0)}{\tan\sigma(0)} \times 100, \tag{3}$$

where $\tan\sigma = \varepsilon'' - \varepsilon'$, ε' is the real part of the dielectric constant, and ε'' is the imaginary part. The low $\tan\sigma$ degree reflects that ceramics were more saturated with little leakage current, which was the major factor for

TABLE I. The magnetodielectric response, magnetodielectric loss, magnetoelectric current, magnetoelectric polarization, and magnetoelectric coupling coefficients of $BaSrCo_{2-x}Cu_xFe_{11}AlO_{22}$ in the low temperature of 78 K. The leakage current and resistivity of the investigated samples in the low temperature of 78 K and room temperature of 300 K.

$BaSrCo_{2x}Cu_xFe_{11}AlO_{22}$	$x = 0$	$x = 0.1$	$x = 0.3$	$x = 0.5$	$x = 0.7$	$x = 0.9$
Magnetodielectric loss (78 K)	0.06	0.01	0.002	0.003	0.002	0.004
$\Delta(\varepsilon)/\varepsilon$(20 kOe)	0.28%	0.58%	0.33%	0.33%	0.19%	0.22%
I ($\mu A/m^2$)	7	8	8	23	15	4
P ($\mu C/m^2$)	10	7	8	35	23	9
dP/dH (ps/m)	1136	1658	1547	4496	2442	753
I_L ($\mu A/cm^2$) (78 K)	8.1×10^{-1}	4.25×10^{-2}	5.67×10^{-4}	1.67×10^{-3}	4.37×10^{-3}	7.12×10^{-3}
Resistivity (Ω cm) (78 K)	2.58×10^{7}	1.07×10^{10}	7.22×10^{11}	2.31×10^{11}	9.96×10^{10}	5.40×10^{10}
I_L ($\mu A/cm^2$) (300 K)	1.29×10^{4}	2.23×10^{3}	2.02×10^{2}	2.28×10^{2}	6.27×10^{2}	7.16×10^{2}
Resistivity (Ω cm) (300 K)	1.47×10^{5}	8.64×10^{5}	5.17×10^{7}	4.51×10^{7}	3.60×10^{7}	1.21×10^{7}

magnetoelectric performance measurements. The ML of $BaSrCo_{2-x}Cu_xFe_{11}AlO_{22}$ was quite low, and when the Cu^{2+} was introduced, the ML value first greatly decreased and then keeps a similar order following the trend shown in Table I [$x = 0$ (0.06) > $x = 0.1$ (0.01) > $x = 0.9$ (0.004) > $x = 0.5$ (0.003) > $x = 0.7/0.3$ (0.002)]. A lower ML value means that samples have very small leakage current. The measured leakage current of $BaSrCo_{2-x}Cu_xFe_{11}AlO_{22}$ under a low temperature of 78 K is in the following trend: $x = 0$ (8.1×10^{-1} $\mu A/cm^2$) > $x = 0.1$ (4.25×10^{-2} $\mu A/cm^2$) > $x = 0.9$ (7.12×10^{-3} $\mu A/cm^2$) > $x = 0.7$ (4.37×10^{-3} $\mu A/cm^2$) > $x = 0.5$ (1.67×10^{-3} $\mu A/cm^2$) > $x = 0.3$ (5.67×10^{-4} $\mu A/cm^2$). The trend of measured leakage current is nearly in accordance with the magnetodielectric loss by the increasing of doped Cu^{2+}. From the magnetodielectric and leakage current performance, it can be inferred when the doped Cu^{2+} over 0.3 benefits the improvement of the samples' insulation degree. The doped Cu^{2+} less than 0.5 benefits the samples' magnetodielectric response. Therefore, the introduced moderate Cu^{2+} is beneficial for the improvement of the samples' degree of insulation and magnetodielectric response, thus benefiting the samples' magnetoelectric coupling performance.

Although the trend of leakage current in room temperature (300 K) is in accordance with the leakage current in low temperature (78 K) as shown in Fig. 5 and Table I, the samples' leakage current in room temperature (300 K) is several orders higher than low temperature (78 K). The samples in room temperature (300 K) are not iusulated enough to guarantee the poling process for magnetoelectric coupling performance measurements due to the large leakage current. So, all investigated samples do not have magnetoelectric coupling performance in room temperature (300 K).

Magnetoelectric features directly reflect the coexistence of ferroelectricity and magnetism, thus demonstrating the multiferroic nature of $BaSrCo_{2-x}Cu_xFe_{11}AlO_{22}$ [30]. Before ME measurements, poling treatments are required for the specimens. First, an external magnetic field (20 kOe) and electric field strength 1 MV/m were applied to the specimens with the direction of the external magnetic field parallel to the surfaces of the prepared specimens for about 1 h in the ceramic's paraelectric phase. Second, the magnetic field was decreased to 2 kOe and the electric field was turned off in the ceramic's ferroelectric phase. Then, the two electrodes of the specimens were short-circuited for about 1 h to release the excess charges. During the ME current measurements, the

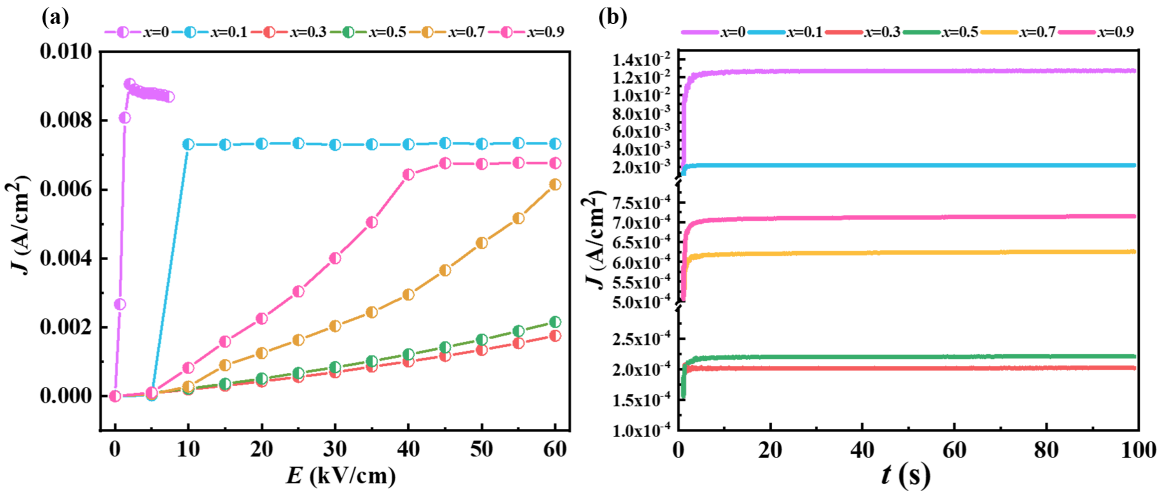

FIG. 5. The leakage current changing with the increase of electric field (a) and the leakage current under stable electric fields of 1 MV/m (b).

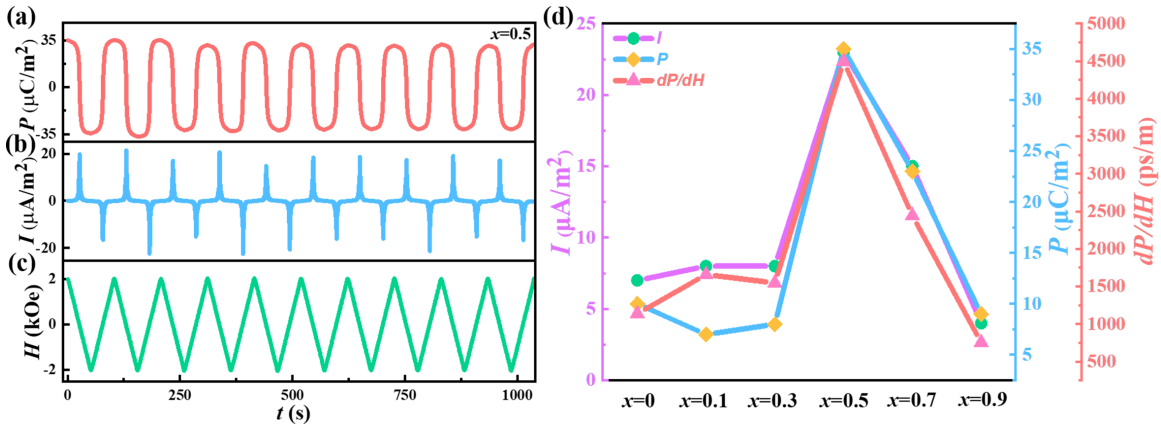

FIG. 6. The reverse of magnetoelectric current (a) and polarization (b) with the periodic circulating magnetic field. (c) The reverse of the outer magnetic field between 2 kOe and −2 kOe. (d) The magnetoelectric current, polarization, and coupling coefficients of $BaSrCo_{2-x}Cu_xFe_{11}AlO_{22}$.

field sweeping program was set between −2 and 2 kOe with the rate of 80 Oe/s.

The ME currents of $BaSrCo_{2-x}Cu_xFe_{11}AlO_{22}$ in Fig. 6(b) exhibit sharp peaks under zero magnetic field, which demonstrated that magnetically controllable ferroelectricity occurred in $BaSrCo_{2-x}Cu_xFe_{11}AlO_{22}$ at 78 K. The magnetoelectric polarization can be obtained by integrating the ME currents with time expressed [31] as

$$P = \int I dt. \tag{4}$$

The magnetoelectric coupling coefficients (α) can be obtained by the derivative of P with respect to H according to the definition [32]

$$\alpha = \frac{dP}{dH}. \tag{5}$$

It was found that introducing Cu^{2+} into the ceramic effectively tuned the magnetoelectric coupling in $BaSrCo_{2-x}Cu_xFe_{11}AlO_{22}$. When $x < 0.5$, the ME currents of $BaSrCo_{2-x}Cu_xFe_{11}AlO_{22}$ ($x < 0.5$) increased compared with $BaSrCo_2Fe_{11}AlO_{22}$. When $x = 0.5$, $BaSrCo_{1.5}Cu_{0.5}Fe_{11}AlO_{22}$ showed the largest ME current of $23\,\mu A/m^2$ as shown in Fig. 6(d) and Table I. When $x > 0.5$, the ME currents of $BaSrCo_{2-x}Cu_xFe_{11}AlO_{22}$ trended lower more gradually than the ME currents of $BaSrCo_{1.5}Cu_{0.5}Fe_{11}AlO_{22}$. Owing to the excellent ME currents in $BaSrCo_{1.5}Cu_{0.5}Fe_{11}AlO_{22}$, the largest magnetoelectric polarization of $35\,\mu C/m^2$ was achieved in $BaSrCo_{1.5}Cu_{0.5}Fe_{11}AlO_{22}$ as shown in Figs. 4(b) and 6(d). It is exciting to see that the polarization changed rapidly around the coercive fields [33], and the maximum magnetoelectric coefficient of $\alpha = 4496 ps/m$ was obtained approaching to zero magnetic field in $BaSrCo_{1.5}Cu_{0.5}Fe_{11}AlO_{22}$ as shown in Figs. 4(c) and 6(d).

Such a low magnetic field induced magnetoelectric performance makes the ceramic promising in practical applications. Many crystals showed excellent magnetoelectric polarization performance under high magnetic fields [8,33–44] as presented in Supplemental Material Table S3 [22]. For example, as reported by Kim *et al.*, the occurring magnetoelectric coupling performance of Ni_3TeO_6 needs a magnetic field up to 520 kOe [34], which was undesirable for the material's application. The prepared *Y*-type $BaSrCo_{1.5}Cu_{0.5}Fe_{11}AlO_{22}$ only requires such low external magnetic field (around 2 kOe) to induce an excellent magnetoelectric current of $23\,\mu A/m^2$, magnetoelectric polarization of $35\,\mu C/m^2$, and magnetoelectric coupling coefficients of 4496 ps/m in the low temperature of 78 K. $BaSrCo_{1.5}Cu_{0.5}Fe_{11}AlO_{22}$ could be applied to conceive and design magnetoelectric functional devices.

The ME current and P in Figs. 6(a), 6(b), and Supplemental Material Figs. S8 and S9 [22] exhibited a flipping feature by reversing the external magnetic field back and forth. Moreover, the ME current and P presented symmetrical switching performance under a periodically alternating magnetic field up to 2 kOe at 78 K. The direction of P also changed with reversing the external magnetic field, shown in Fig. 4(b). P of $BaSrCo_{2-x}Cu_xFe_{11}AlO_{22}$ changed rapidly in the low-H region (below 2 kOe), corresponding to the paraelectric to ferroelectric phase transition with decreasing external magnetic field. The peaks of ME currents (see Supplemental Material Fig. S6 [22]) around zero magnetic field were proof of transition from paraelectric to ferroelectric phases, which can be explained changes in magnetic structures. One sees that under a relatively high magnetic field range (2–20 kOe), the samples were apparently with collinear ferromagnetic structure, which cannot induce the magnetoelectric current (see Supplemental Material Fig. S8 [22]), therefore, materials stay in the paraelectric phase. With the magnetic field decreasing to near 2 kOe, the ceramics seem to be in longitudinal conical magnetic structure, which cannot evoke the magnetoelectric current, thus, the hexaferrites also remain in their paraelectric phase. The specimen's magnetic structures gradually transition to transverse-conical screw under zero magnetic field, which can induce the maximum magnetoelectric current, namely, the samples remain in their ferroelectric phase. It was noted that magnetoelectric polarization experiences fatigue attenuation. In order to further illustrate the relationship of maximum polarization with the sweeping times of magnetic fields, the P decaying feature in $BaSrCo_{2-x}Cu_xFe_{11}AlO_{22}$ was fitted to

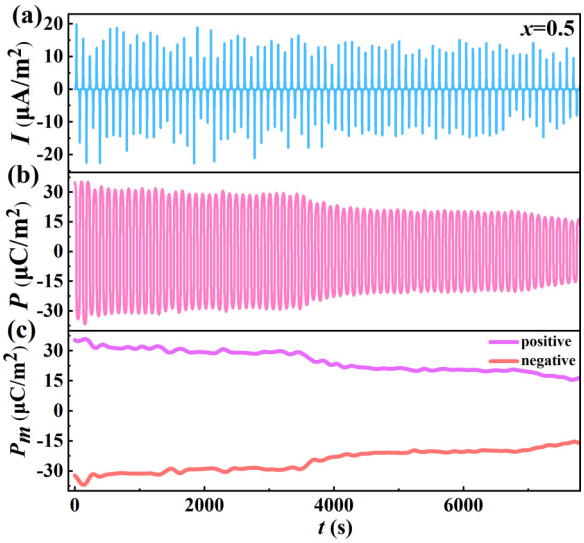

FIG. 7. The decayless magnetoelectric current (a) and magnetoelectric polarization (b) of $BaSrCo_{1.5}Cu_{0.5}Fe_{11}AlO_{22}$. (c) The decayless maximum magetoelectric polarization value.

the decaying curves in Fig. 7 and Supplemental Material Fig. S10 [22] by the following expression [45]:

$$P_m = P_{m0} + A_m e^{-n/t_m}, \tag{6}$$

where P_m represents the maximum polarization value, P_{m0} is a constant, and A_m and t_m represent the attenuation constants with the cycling times (n). The fitted curves were depicted in Supplemental Material Fig. S11 [22]. The fatigue attenuation phenomenon exhibited frustrated behaviors with increasing Cu^{2+}. The frustrated decreasing trend occurred in $BaSrCo_{1.1}Cu_{0.9}Fe_{11}AlO_{22}$ and was fitted to the following formula:

$$y = 1.40 + 7.01e^{(-x/15.10)}. \tag{7}$$

Although the $BaSrCo_{1.1}Cu_{0.9}Fe_{11}AlO_{22}$ composition exhibited the worst frustrated attenuation, the P value in $BaSrCo_{1.1}Cu_{0.9}Fe_{11}AlO_{22}$ tended to a constant of 1.4 $\mu C/m^2$, when sweeping cycles n tended to infinity with the increasing of magnetic fields. This demonstrated that the P reversion still exists, namely, such reversion is intrinsic in $BaSrCo_{2-x}Cu_xFe_{11}AlO_{22}$, with as high as 14.9 $\mu C/m^2$ polarization value with the sweeping cycles approaching to infinity.

Magnetoelectric polarization versus external magnetic field at different angle (θ) between the direction of the electrodes' surfaces and the external magnetic field are depicted in Fig. 8 and Supplemental Material Fig. S12 [22].

The schematic diagram for the measurements of magnetoelectric polarization changing with angle (θ) is vividly depicted in Supplemental Material Fig. S13 [22]. It is seen that magnetoelectric polarization gradually decreased with the angle changing from 0° to 90°, reaching the least polatization value at 90°. And then, the magnetoelectric polarization gradually increased in the opposite direction with the angle changing from 90° to 180°. It is noted that magnetoelectric polarization in the angles range of 180°–360° showed similar behavior as that for the angle range from 0° to 180°. It is no surprise that the least polarization value was when the magnetic field was perpendicular to the two electrodes. Such an angle dependence no doubt offers flexibility in practical applications.

C. The impact of Cu^{2+} doping on magnetoelectric performances of $BaSrCo_{2-x}Cu_xFe_{11}AlO_{22}$

As aforementioned, introducing Cu^{2+} to the $BaSrCo_{2-x}Cu_xFe_{11}AlO_{22}$ $(0 < x < 1)$ ceramics has a significant influence on its ME performance, which can be experimentally demonstrated by the samples' magnetodielectric performance, leakage current, and magnetoelectric polarization performance [3].

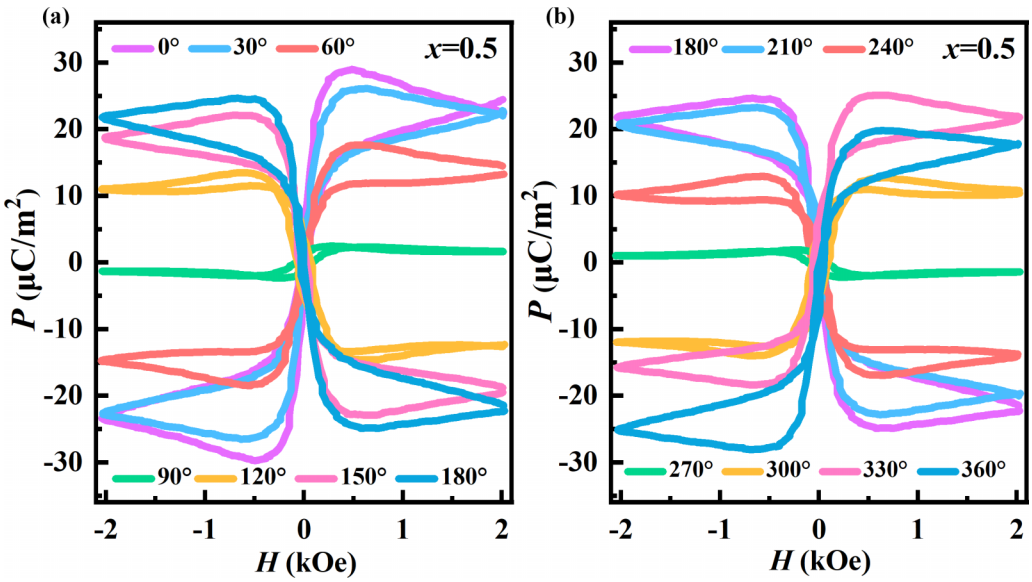

FIG. 8. The magnetoelectric polarization changing with angles between the direction of electrodes connection and external magnetic field in $BaSrCo_{1.5}Cu_{0.5}Fe_{11}AlO_{22}$ corresponding to the angles between (a) 0° and 180° and (b) 180° and 360°.

First, compared with $BaSrCo_2Fe_{11}AlO_{22}$, the samples' ML greatly decreased when the doped Cu^{2+} was over 0.3. So, the samples' insulation degree was enhanced, which benefits the samples' magnetoelectric coupling performance. When the doped Cu^{2+} was over 0.5, the samples' magnetodielectric response degree decreased, which was not beneficial for the samples' magnetoelectric coupling performances. The samples' insulation degree first greatly decreased ($x < 0.3$) and then gradually increased ($x > 0.5$) reflected by the first greatly decreased leakage current ($x < 0.3$) and the gradually increased leakage current ($x > 0.5$). The large insulation degree benefits the samples' magnetoelectric coupling performance. So, from the samples' magnetodielectric and leakage current performances, the introduced moderately doped Cu^{2+} benefits the improvement of the samples' insulation degree and magnetodielectric response to contribute to the samples' magnetoelectric polarization performances.

Furthermore, P can also be enhanced with the properly doped Cu^{2+} ($x < 0.5$). For $x = 0.5$, the largest P was also obtained in $BaSrCo_{1.5}Cu_{0.5}Fe_{11}AlO_{22}$. Once raising the doping Cu^{2+} concentration further beyond $x > 0.5$, the P value in $BaSrCo_{2-x}Cu_xFe_{11}AlO_{22}$ gradually decreased. It is quite exciting to the samples' excellent magnetodielectric performance, and the samples' low leakage current and large magnetoelectric polarization performances occurred at the Cu^{2+}-doped composition of $x = 0.5$.

In fact, the magnetoelectric polarization can be determined by the inverse Dzyaloshinsky-Moriya interaction mechanism by the following expression [46]:

$$P = A\alpha \sum_{ij} \vec{k} \times \vec{\mu_L} \times \vec{\mu_S}, \tag{8}$$

where $\vec{k}$ is the propagation vector and A is a scalar determined by the superexchange interaction [46]. The interaction coefficient (A) has a proportional relationship with the interaction effects of $\vec{\mu_L}$ and $\vec{\mu_S}$ [44]. Therefore, P is proportional to A and the magnetic moments. With the increase of Cu^{2+} (decrease of Co^{2+}), the crystal's magnetic moments gradually decreased, reflected by the decreasing saturation magnetization in Figs. 2(b) and 2(c), which were undesirable for the magnetoelectric polarization performances. However, when the doped Cu^{2+} was up to $x = 0.5$, $BaSrCo_{1.5}Cu_{0.5}Fe_{11}AlO_{22}$ exhibited the largest magnetoelectric polarization. Compared with $BaSrCo_2Fe_{11}AlO_{22}$, $BaSrCo_{1.5}Cu_{0.5}Fe_{11}AlO_{22}$ exhibited reduced magnetic moments while increased P. According to expression (8), the enhanced P can be attributed to the enhanced A between magnetic moments. The enhanced A may be owing to the smaller radius Cu^{2+} (0.73 Å) compared with the large radius Co^{2+} (0.745 Å), leading to the dense crystal structure, confirmed by the decreasing constants and cell volume according to the increased diffraction angles by equation $2d \sin\theta = n\lambda$ [47]. For instance, the diffraction angles of (220) in Supplemental Material Fig. S1 [22] presented an increasing trend with increasing Cu^{2+}, suggesting the lattice constants gradually decrease with increasing Cu^{2+}. Such decreasing lattice constants and cell volume can result in dense ceramics and make the adjacent S and T blocks closer. The densification of the T and S blocks can in turn contribute to the enhancement of the superexchange interaction between $\vec{\mu_L}$ and $\vec{\mu_S}$, and hence leads to the enhanced ME coupling performances reported by Zhai *et al.* [9]. Therefore, it can be concluded that the enhancement of P in $BaSrCo_{1.5}Cu_{0.5}Fe_{11}AlO_{22}$ can be at least partially attributed to the doping of Cu^{2+} with a smaller radius (0.73 Å), by substituting the Co^{2+} with a large radius (0.745 Å). The enhanced superexchange interaction then resulted in the improvement of the ceramic's P. However, oversubstitution of Co^{2+} with Cu^{2+} can cause decreasing macromagnetization, which is not expedient for the enhancement of P. At doping ratio $x = 0.5$, optimized magnetoelectric polarization performances were reached in $BaSrCo_{1.5}Cu_{0.5}Fe_{11}AlO_{22}$, with maximum magnetoelectric coupling coefficients of 4496 ps/m.

IV. CONCLUSION

To summarize, Cu^{2+}-doped Y-type $BaSrCo_{2-x}Cu_xFe_{11}AlO_{22}$ ($0 < x < 1$) ceramics were first prepared, witnessing great decreasing ceramic leakage current and strengthening the hexaferrites' magnetoelectric coupling upon introducing Cu^{2+} and substituting Co^{2+}. Tunable magnetoelectric polarization was observed in $BaSrCo_{2-x}Cu_xFe_{11}AlO_{22}$ realized under one magnitude of order lower magnetic field, with reversibility associated with external magnetic fields. By changing the angles between the surfaces of two electrodes and the external magnetic field, magnetoelectric polarization intensity can be manipulated. It is found that Cu^{2+} substituting for Co^{2+} led to decreasing magnetization in $BaSrCo_{2-x}Cu_xFe_{11}AlO_{22}$. External magnetic field induced P exhibited fatigue attenuation behavior, frustrated with increasing Cu^{2+}. The samples' insulation and magnetodielectric response degree enhanced by moderately doped Cu^{2+} are reflected by the decreased leakage current, magnetodielectric loss, and enhanced magnetodielectric response, which contributes to the samples' magnetoelectric coupling performance. Further, it is evidenced that introducing Cu^{2+} with a smaller radius (0.73 Å) to replace Co^{2+} with a large radius (0.745 Å) shortens the distance between the T and S blocks. Such a densification between the T and S blocks can enhance the superexchange interaction between the magnetic moments of $\vec{\mu_L}$ and $\vec{\mu_S}$, which is believed to be behind the enhanced P, especially for the composition $BaSrCo_{1.5}Cu_{0.5}Fe_{11}AlO_{22}$. The excellent combination of a magnetoelectric current of 23 $\mu A/m^2$, P of 35 $\mu C/m^2$, and maximum magnetoelectric coupling coefficients of 4496 ps/m obatained in $BaSrCo_{1.5}Cu_{0.5}Fe_{11}AlO_{22}$ make this family of magnetoelectric Y-type hexaferrites highly promising in practical applications in designing nonvolatile memory devices.

The data that support the findings of this study are available from the corresponding author upon reasonable request.

ACKNOWLEDGMENTS

This work was supported by the National Natural Science Foundation of China (Grants No. U2130110 and No. 51502054) and Fundamental Research Funds for the Central Universities (Project No. 2023FRFK06003).

The authors declare no conflict of interest.

[1] X. Wang, Y. S. Chai, L. Zhou, H. B. Cao, C. D. Cruz, J. Y. Yang, J. H. Dai, Y. Y. Yin, Z. Yuan, S. J. Zhang, R. Z. Yu, M. Azuma, Y. C.Shimakawa, H. M. Zhang, S. Dong, Y. Sun, C. Q. Jin, and Y. W. Long, Observation of magnetoelectric multiferroicity in a cubic perovskite system: $LaMn_3Cr_4O_{12}$, Phys. Rev. Lett. **115**, 087601 (2015).

[2] Y. Tokura and S. Seki, Multiferroics with spiral spin orders, Adv. Mater. **22**, 1554 (2010).

[3] M. Adnani, M. Gooch, L. Z. Deng, S. Agrestini, J. Herrero-Martin, H. C. Wu, C. K. Chang, T. Salavati-fard, N. Poudel, J. L. García-Muñoz, S. Daneshmandi, Z. Wu, L. C. Grabow, Y. C. Lai, H. D. Yang, E. Pellegrin, and C. W. Chu, Magnetocapacitance effect and magnetoelectric coupling in type-II multiferroic $HoFeWO_6$, Phys. Rev. B **103**, 094110 (2021).

[4] H. M. Jang, J. H. Park, S. W. Ryu, and S. R. Shannigrahi, Magnetoelectric coupling susceptibility from magnetodielectric effect, Appl. Phys. Lett. **93**, 252904 (2008).

[5] M. Soda, T. Ishikura, H. Nakamura, Y. Wakabayashi, and T. Kimura, Magnetic ordering in relation to the room-temperature magnetoelectric effect of $Sr_3Co_2Fe_{24}O_{41}$, Phys. Rev. Lett. **106**, 087201 (2011).

[6] S. Ishiwata, Y. Taguchi, H. Murakawa, Y. Onose, and Y. Tokura, Low-magnetic-field control of electric polarization vector in a helimagnet, Science **319**, 1643 (2008).

[7] K. Taniguchi, N. Abe, S. Ohtani, H. Umestu, and T. Arima, Ferroelectric polarization reversal by a magnetic field in multiferroic Y-type hexaferrite $Ba_2Mg_2Fe_{12}O_{22}$, Appl. Phys. Exp. **1**, 031301 (2008).

[8] S. Hirose, K. Haruki, A. Ando, and T. Kimura, Effect of high-pressure oxygen annealing on electrical and magnetoelectric properties of $BaSrCo_2Fe_{11}AlO_{22}$ ceramics, J. Am. Ceram. Soc. **98**, 2104 (2015).

[9] K. Zhai, Y. Wu, S. P. Shen, W. Tian, H. B. Cao, Y. S. Chai, B. C. Chakoumakos, D. Shang, L. Q. Yan, F. W. Wang, and Y. Sun, Giant magnetoelectric effects achieved by tuning spin cone symmetry in Y-type hexaferrites, Nat. Commun. **8**, 519 (2017).

[10] S. Hirose, K. Haruki, A. Ando, and T. Kimura, Mutual control of magnetization and electrical polarization by electric and magnetic fields at room temperature in Y-type $BaSrCo_{2-x}Zn_xFe_{11}AlO_{22}$ ceramics, Appl. Phys. Lett. **104**, 022907 (2014).

[11] S. H. Chun, Y. S. Chai, Y. S. Oh, D. Jaiswal-Nagar, S. Y. Haam, I. Kim, B. Lee, D. H. Nam, K. T. Ko, J. H. Park, J. H. Chung, and K. H. Kim, Realization of giant magnetoelectricity in helimagnets, Phys. Rev. Lett. **104**, 037204 (2010).

[12] S. Hirose, D. Urushihara, T. Asaka, and T. Kimura, Improved room-temperature magnetoelectric effect and crystal structure in polycrystalline $BaSrCo_2Fe_{11}AlO_{22}$, Appl. Phys. Lett. **118**, 062407 (2021).

[13] M. F. Abdullah, P. Pal, K. Chandrakanta, R. Jena, S. Devi, C. S. Yadav, and A. K. Singh, Enhanced magnetic and room temperature intrinsic magnetodielectric effect in Mn modified $Ba_2Mg_2Fe_{12}O_{22}$ Y-type hexaferrite, J. Phys.: Condens. Matter **32**, 135701 (2020).

[14] C. B. Park, K. W. Shin, S. H. Chun, J. H. Lee, Y. S. Oh, S. M. Disseler, C. A. Heikes, W. D. Ratcliff, W. S. Noh, J. H. Park, and K. H. Kim, Control of magnetoelectric coupling in the Co_2 Y-type hexaferrites, Phys. Rev. Mater. **5**, 034412 (2021).

[15] C. Xu, A. L. Zhang, Z. J. Feng, W. L. Lu, B. J. Kang, J. C. Zhang, J. Y. Ge, and S. X. Cao, Spin-orbit coupling in magnetoelectric $Ba_3(Zn_{1-x}Co_x)_2Fe_{24}O_{41}$ hexaferrites, Phys. Chem. Chem. Phys. **21**, 25826 (2019).

[16] R. J. Tang, H. Zhou, W. L.You, and H. Yang, Room-temperature multiferroic and magnetocapacitance effects in M-type hexaferrite $BaFe_{10.2}Sc_{1.8}O_{19}$, Appl. Phys. Lett. **109**, 082903 (2016).

[17] K. T. Ko, M. H. Jung, Q. He, J. H. Lee, C. S. Woo, K. Chu, J. Seidel, B. G. Jeon, Y. S. Oh, K. H. Kim, W. I. Liang, H. J. Chen, Y. H. Chu, Y. H. Jeong, R. Ramesh, J. H. Park, and C. H. Yang, Concurrent transition of ferroelectric and magnetic ordering near room temperature, Nat Commun. **2**, 567 (2011).

[18] F. Wang, S. P. Shen, and Y. Sun, Magnetoelectric memory effect in the Y-type hexaferrite $BaSrZnMgFe_{12}O_{22}$, Chin. Phys. B **25**, 087503 (2016).

[19] X. Wang, Z. J. Su, A. Sokolov, B. L. Hu, P. Andalib, Y. J. Chen, and V. G. Harris, Giant magnetoresistance due to magnetoelectric currents in $Sr_3Co_2Fe_{24}O_{41}$ hexaferrites, Appl. Phys. Lett. **105**, 112408 (2014).

[20] H. B. Lee, Y. S. Song, J. H. Chung, S. H. Chun, Y. S. Chai, K. H. Kim, M. Reehuis, K. Prokeš, and S. Mat'aš, Field-induced incommensurate-to-commensurate phase transition in the magnetoelectric hexaferrite $Ba_{0.5}Sr_{1.5}Zn_2(Fe_{1-x}Al_x)_{12}O_{22}$, Phys. Rev. B **83**, 144425 (2011).

[21] P. Novák, K. Knížek, and J. Rusz, Magnetism in the magnetoelectric hexaferrite system $(Ba_{1-x}Sr_x)_2Zn_2Fe_{12}O_{22}$, Phys Rev. B **76**, 024432 (2007).

[22] See Supplemental Material at http://link.aps.org/supplemental/10.1103/PhysRevB.108.184430 for the details of elements occupation percentage; the reported materials' magnetoelectric performance; the main XRD peaks shift; the morphology and phase; the dielectric, magnetic, and magnetoelectric coupling performances; and the schematic diagram for the magnetoelectric coupling performance with angles. It also contains Refs. [8,33–44].

[23] Y. Hiraoka, H. Nakamura, M. Soda,Y. Wakabayashi, and T. Kimura, Magnetic and magnetoelectric properties of $Ba_{2-x}Sr_xNi_2Fe_{12}O_{22}$ single crystals with Y-type hexaferrite, J. Appl. Phys. **110**, 033920 (2011).

[24] L. Z. Ji, R. Z. Zhao, X. Hu, C. L. Hu, X. C. Shen, X. L. Liu, X. Y. Zhao, J. Zhang, W. C. Chen, and X. F. Zhang, Reconfigurable ferromagnetic resonances by engineering inhomogeneous magnetic textures in artificial magnonic crystals, Adv. Funct. Mater. **32**, 2112956 (2022).

[25] Y. F. Chang, K. Zhai, and Y. Sun, Magnetoelectric effects in multiferroic Y-type hexaferrites $Ba_{0.3}Sr_{1.7}Co_xMg_{2-x}Fe_{12}O_{22}$, Chin. Phys. B **29**, 037701 (2020).

[26] L. Chen and Y. Wang, The effects of the soft magnetic alloys' material characteristics on resonant magnetoelectric coupling for magnetostrictive/piezoelectric composites, Smart Mater. Struct. **28**, 045003 (2019).

[27] H. B. Lee, S. H.Chun, K. W. Shin, B. G. Jeon, Y. S. Chai, K. H. Kim, J. Schefer, H. Chang, S. N. Yun, T. Y. Joung, and J. H. Chung, Heliconical magnetic order and field-induced multiferroicity of the Co_2 Y-type hexaferrite $Ba_{0.3}Sr_{1.7}Co_2Fe_{12}O_{22}$, Phys Rev. B **86**, 094435 (2012).

[28] K. Okumura, K. Haruki, T. Ishikura, S. Hirose, and T. Kimura, Multilevel magnetization switching by electric field in c-axis oriented polycrystalline Z-type hexaferrite, Appl. Phys. Lett. **103**, 032906 (2013).

[29] G. Catalana, Magnetocapacitance without magnetoelectric coupling, Appl. Phys. Lett. **88**, 102902 (2006).

[30] S. H. Chun, K. W. Shin, H. J. Kim, S. Jung, J. Park, Y. M. Bahk, H. R. Park, J. Kyoung, D. H. Choi, D. S. Kim, G. S. Park, J. F. Mitchell, and K. H. Kim, Electromagnon with sensitive terahertz magnetochromism in a room-temperature magnetoelectric hexaferrite, Phys. Rev. Lett. **120**, 027202 (2018).

[31] H. Katsura, N. Nagaosa, and A. V. Balatsky, Spin current and magnetoelectric effect in noncollinear magnets, Phys. Rev. Lett. **95**, 057205 (2005).

[32] W. Eerenstein, N. D. Mathur, and J. F. Scott, Multiferroic and magnetoelectric materials, Nature **442**, 759 (2006).

[33] S. P. Shen, L. Q. Yan, Y. S. Chai, J. Z. Cong, and Y. Sun, Magnetic field reversal of electric polarization and magnetoelectric phase diagram of the hexaferrite $Ba_{1.3}Sr_{0.7}Co_{0.9}Zn_{1.1}Fe_{10.8}Al_{1.2}O_{22}$, Appl. Phys. Lett. **104**, 032905 (2014).

[34] J. W. Kim, S. Artyukhin, E. D. Mun, M. Jaime, N. Harrison, A. Hansen, J. J. Yang, Y. S. Oh, D. Vanderbilt, V. S. Zapf, and S. W. Cheong, Successive magnetic-field-induced transitions and colossal magnetoelectric effect in Ni_3TeO_6, Phys. Rev. Lett. **115**, 137201 (2015).

[35] T. Kurumaji, S. Ishiwata, and Y. Tokura, Doping-tunable ferrimagnetic phase with large linear magnetoelectric effect in a polar magnet $Fe_2Mo_3O_8$, Phys Rev. X **5**, 031034 (2015).

[36] T. Kimura, G. Lawes, T. Goto, Y. Tokura, and A. P. Ramirez, Magnetoelectric phase diagrams of orthorhombic RMnO$_3$ (R=Gd, Tb, and Dy), Phys Rev. B **71**, 224425 (2005).

[37] G. Z. Zhou, J. W. Gong, X. Li, M. F. Liu, L. Y. Li, Y. Wang, J. H. Min, J. Liu, D. Cai, F. Liu, S. H. Zheng, Y. S. Tang, Z. C. Xu, Y. L. Xie, L. Yang, M. Zeng, Z. B. Yan, B. W. Li, X. Z. Wang, and J. M. Liu, Large magnetoelectric effect in the polar magnet Sm_2BaCuO_5, Appl. Phys. Lett. **115**, 252902 (2019).

[38] T. Aoyama, A. Iyama, K. Shimizu, and T. Kimura, Multiferroicity in orthorhombic RMnO$_3$ (R=Dy,Tb, and Gd) under high pressure, Phys Rev. B **91**, 081107(R) (2015).

[39] N. Lee, C. Vecchini, Y. J. Choi, L. C. Chapon, A. Bombardi, P. G. Radaelli, and S. W. Cheong, Giant tunability of ferroelectric polarization in $GdMn_2O_5$, Phys. Rev. Lett. **110**, 137203 (2013).

[40] H. Murakawa, Y. Onose, K. Ohgushi, S. Ishiwata, and Y. Tokura, Generation of electric polarization with rotating magnetic field in helimagnet $ZnCr_2Se_4$, J. Phys. Soc. Jpn. **77**, 043709 (2008).

[41] P. Z. Li, W. Wang, K. Cheng, J. Li, J. B. Xian, C. A. Wang, C. M. Leung, M. F. Liu, and M. Zeng, Direct evidence of mutual control of ferroelectric polarization and magnetization in Y-type hexaferrite $BaSrCo_2Fe_{12-x}Al_xO_{22}$ ceramics, J. Alloys Compd. **911**, 165121 (2022).

[42] C. K. Wang, C. Xu, X. X. Ma, H. Y. Chen, W. C. Fan, F. Chen, B. J. Kang, J. Y. Ge, W. Ren, and S. X. Cao, Magnetoelectric coupling in $Sr_3Co_2Fe_{23.04}Al_{0.96}O_{41}$ single crystal near room temperature, J. Alloys Compd. **905**, 164233 (2022).

[43] C. S. Wu, Q. Liu, Y. Wang, J. F. Chen, B. H. Qi, H. W. Zhang, and Y. L. Liu, Room-temperature nonvolatile four-state memory based on multiferroic $Sr_3Co_2Fe_{21.6}O_{37.4}$, J. Alloy. Compd. **779**, 115 (2019).

[44] C. S. Wu, Q. Liu, Y. Wang, B. H. Qi, H. W. Zhang, and Y. L. Liu, Effect of scanning magnetic field on the spiral magnetic structure of magnetoelectric hexaferrite $Sr_3Co_2Fe_{24}O_{41}$, Ceram Int. **44**, 19695 (2018).

[45] K. Ebnabbasi, C. Vittoria, and A. Widom, Converse magnetoelectric experiments on a room-temperature spirally ordered hexaferrite, Phys Rev. B **86**, 024430 (2012).

[46] C. A. F. Vaz, J. Hoffman, C. H. Ahb, and R. Ramesh, Magnetoelectric coupling effects in multiferroic complex oxide composite structures, Adv. Mater. **22**, 2900 (2010).

[47] X. H. Chen, K. Zhai, G. Y. Qian, Q. S. Fu, C. Chakrabarti, C. L. Li, H. X. Yin, Y. Qiu, Z. M. Tian, and S. L. Yuan, Enhanced room-temperature magnetoelectric coupling effects in c-axis oriented polycrystalline $BaSrCo_{2-x}Mg_xFe_{11}AlO_{22}$, J. Am. Ceram. Soc. **104**, 3334 (2021).